Critical heat flux enhancement regarding to the thickness of graphene films under pool boiling

Jin Man Kim [a], Youngjae Park [b], Hyungdae Kim [b], Dong Eok Kim[c], Hyun Sun Park [a], Moo Hwan Kim [d], Ho Seon Ahn [e*]
[a]*Div. of Adv. Nuclear Engr., Pohang Univ. of Science and Technology, 77 Cheongam-Ro, Pohang, 790-784*
[b]*Dept. of Nuclear Engr., Kyung Hee Univ., 1732, Deogyeong-daero, Yongin, 449-701*
[c]*Dept. of Precision Mech. Engr., Kyungpook Nat. Univ., 2559 Gyeongsang-daero, Sang ju, 742-711*
[d]*Korea Inst. of Nuclear Safety, 62 Gwahak-ro, Daejeon, 305-338*
[e]*Div. of Mech. System Engr.,Incheon Nat. Univ., 119 Academy-ro, Incheon, 406-772*
[*]*Corresponding author: hsahn@incheon.ac.kr*

1. Introduction

In this study, graphene films of various thicknesses are deposited on a heated surface, and enhancements of BHT and CHF are investigated via pool-boiling experiments. In contrast to the well-known surface effects, including improved wettability and liquid spreading due to micron- and nanometer-scale structures, nanometer-scale folded edges of graphene films provided a clue of BHT improvement and only the thermal conductivity of the graphene layer can explain the dependence of the CHF on the thickness. The large thermal conductivity of the graphene films inhibits the formation of hot spots, thereby increasing the CHF. An infrared high-speed visualization showed graphene effect on boiling characteristics during operation.

2. Methods and Results

To investigate the thickness effect of graphene film on pool boiling characteristics, pool boiling experiments were conducted with infrared high-speed visualization.

2.1 Test section

Figure 1 shows images of the heater used in this work, which consisted of a double-sided polished silicon substrate with a thermally grown silicon dioxide (SiO_2) surface and a deposited platinum thin-film heater. The test heater measured 25 × 20 mm, and effective heating area was 15 × 10 mm with Joule heating method using lead solder wiring. To calibrate the wall temperature, it is important to accurately determine the voltage and current during operation so that the resistance of each test sample can be correlated as a function of the temperature.

For making graphene film, colloidal suspensions of the reduced garphene oxide (RGO) flakes in DI water were prepared at concentrations of 0.001 wt.%. The graphene film was obtained via filtration, which was carried out using a vacuum. A cellulose paper filter with 450-nm-diameter pores was used to filter the RGO flakes from the colloidal suspension. During filtration, the cellulose paper retained the RGO flakes at the surface as the water flowed through the paper, resulting in conformal orientation of the RGO flakes along the filter paper.[1] Following filtration, the graphene film was on the cellulose filter paper, along with absorbed water.

To transfer graphene film on the silicon heater surface, alumina ceramic blocks were used to press the silicon heater and the cellulose paper together using a vice, and placed in an oven at 63°C for 1 hour. The cellulose paper was subsequently peeled off the heater, leaving the graphene film on the heater, as shown in **Figure 1b**. [2]

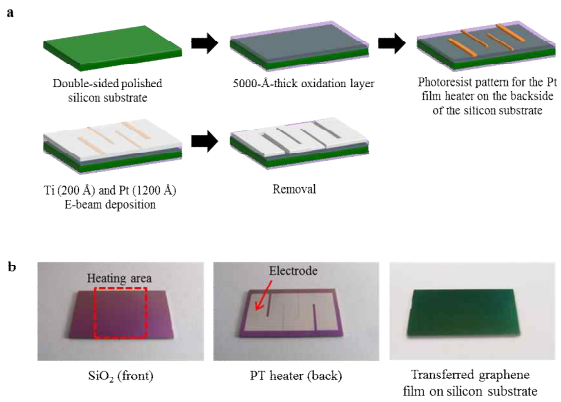

Fig. 1. Silicon heater. **a.** Fabrication of silicon heater. **b.** Pictures of silicon heater images and transferred graphene film on silicon heater. [2]

2.2 Pool boiling facilities

Figure 2a shows a schematic diagram of the experimental pool-boiling facility, which was designed to carry out pool-boiling experiments to measure BHT and the CHF under atmospheric pressure and using Joule heating. The facility operates with a test sample and a main pool chamber. Here, the test sample consisted of a silicon substrate and a polyetheretherketone (PEEK) test sample frame. PEEK is a thermoplastic that has a large thermal resistance and is compatible with an aqueous chemical environment. The test samples were waterproofed and fixed using an adhesive sealant (Permatex clear room-temperature vulcanizing (RTV) silicone), as shown in **Figure 2b**. The main pool chamber was a rectangular bath formed of 10-mm-thick aluminum sheet with a 4-liter capacity. The test sample was located at the bottom of the pool

chamber. A reflux condenser was installed at the top of the main pool chamber to prevent evaporation of the working fluid, which was DI water.

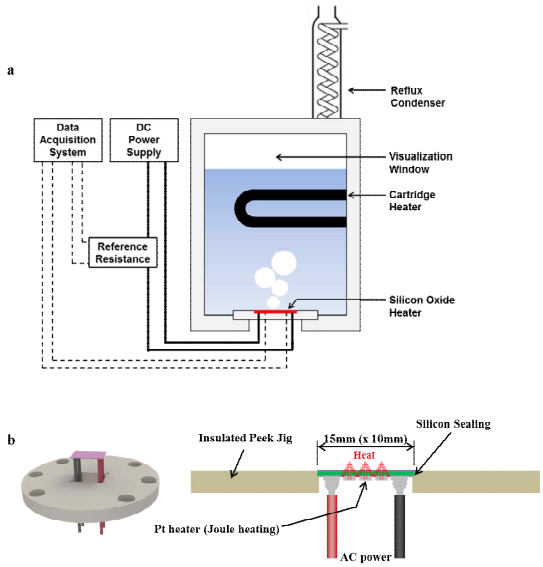

Fig. 2. Pool boiling facilities. **a.** Schematic images of pool and test section. **b.** Test section with silicon heater. [2]

2.3 Pool boiling results

Here, we report that thin graphene films on a heated surface may result in more efficient dissipation of heat in the lateral direction, which inhibits the formation of dry/hot spots during boiling, leading to an increase in the BHT and CHF. The role of graphene films on the heated surface was investigated using infrared high-speed visualization of the boiling process. We found that the graphene layer led to an increase in the CHF and BHT via lateral heat transport, which inhibited the formation of hot/dry spots.

Prior to the boiling experiments, the working fluid was heated in the pool for 1 hour via a submerged cartridge heater for degassing purposes. During the experiments, the heat flux was increased in 100-kWm^{-2} steps, with a 2-minute period for steady-state data acquisition. At heat fluxes of less than 100 kWm^{-2}, a 10-kWm^{-2} step was used to observe the ONB. When the CHF occurred, the wall temperature increased rapidly, at which time the electrical power was shut down to prevent heater failure.

Figure 3 shows the boiling curves of the heated surface with and without the transferred graphene layer. The onset of nucleate boiling (ONB) occurred at a similar point for all the surfaces, and the graphene-coated surfaces exhibited an increase in both BHT and the CHF compared with the bare silicon surface. BHT was more significant on the graphene films than on the bare silicon surface, and accounted for as much as 90%. The BHT component was similar for the 50-, 100-, 150- and 200-nm-thick films; however, the respective CHFs of the four different thickness films were 1102, 1204, 1302 and 1300 kWm^{-2}. The CHF increased with the thickness of the graphene film.

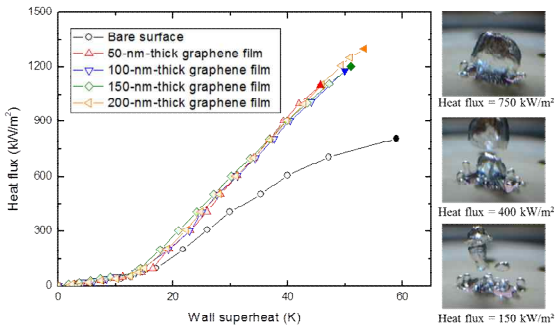

Fig. 3. Boiling curves for all surfaces. [2]

2.4 Analysis

Figure 4a shows static contact angle measurements of the surfaces. The bare silicon surface exhibited a contact angle of 63°, and the surfaces with 100- and 200-nm-thick graphene films exhibited contact angles of 81.9° and 81.5°, respectively. The change in the surface wettability due to the presence of the graphene film cannot explain the increase in the CHF, as there was no significant change in the contact angle as the thickness of the graphene film was varied. However, the slight decrease in wettability compared with the bare silicon surface may enhance BHT because the diameter of departing bubbles during nucleate boiling is expected to decrease. In addition, as shown in **Figure 4b**, the graphene films exhibited nanometer-scale folded edges, where the edges of the upper-most RGO flakes were partially folded; this is consistent with the observations of Bae.[3] It follows that bubble nucleation on the graphene film may occur more readily than on the bare silicon heater because the nanometer-scale folded edges of the RGO flakes may act as nucleation sites. It is conjectured that these edges contributed to improved BHT.

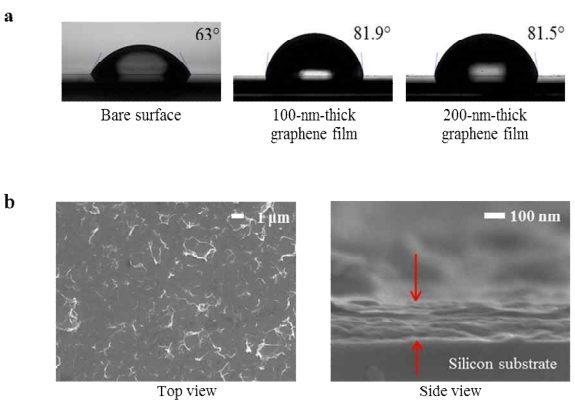

Fig. 4. Surface characteristics. **a.** Contact angles on bare, 100-nm-thick and 200-nm-thick graphene film. **b.** SEM images of the graphene film. [2]

It is well known that an increase in the thermal conductivity of the heated surface can lead to an increase in the CHF. This is due to lateral heat dissipation, which can inhibit the formation of hot spots during nucleate boiling.[4] It has been reported that the density ρ_w, as well as the thermal conductivity k_w, the heat capacity $C_{p,w}$, and the thickness of the heated surface δ_w can all affect the CHF.[5, 6] Arik and Bar Cohen[3] reported that the CHF increases with the thickness of the heated surface, approaching an asymptotic limit. They found that the thermal activity could be described by $S = \delta_w \sqrt{\rho_w C_{p,w} k_w}$, and that the ratio of the CHF q''_{CHF} to the asymptote q''_{max} can described by

$$\frac{q''_{CHF}}{q''_{max}} \propto \frac{S}{S+C} \qquad (1)$$

where the constant C is a fitting parameter. We used a phenomenological relationship between the thermal conductivity of the graphene film and the thickness[7] to calculate the thermal activity. Because the thicknesses of the graphene films were in the range 15–200 nm, the effective thermal conductivity of the graphene films was estimated to be in the range 1000–2000 $W \cdot m^{-1} \cdot K^{-1}$, which can be expressed by

$$k = k_0 + (k_{bulk} - k_0)\left[1 - \frac{2\delta}{t}\tanh\left(\frac{t}{2\delta}\right)\right] \qquad (2)$$

where k_0 is an approximately constant value with zero thickness, k_{bulk} is the thermal conductivity of bulk graphite, δ is the characteristic length, and t is the total thickness of the film.

The thermal capacity and density of graphene were assumed to be the same as those of graphite.[8] As the thickness of the graphene films increased to 150 nm, the CHF increased to 1320 $kW \cdot m^{-2}$. When the thickness of graphene increased beyond 150 nm, no further increase in the CHF was observed. This asymptotic behavior of the CHF as a function of the thickness of the graphene film indicates that the maximum CHF was 1320 $kW \cdot m^{-2}$, which represents a 62.5% increase compared with the bare silicon surface. The thermal conductivity of graphene film is already close to asymptotic value at the 40-nm-thick garphene film. Thus, the increase in the CHF as the thickness varied from 40–200 nm is dependent only on the thickness of the graphene films. We calculated the thermal activity of the graphene films, which were in the range $0 < S < 1$; however, most were of the order of 10–2. The fitting constant was varied in the range $0.0001 < C < 0.001$, as shown in **Figure 5**, which was found to provide good agreement with the experimental data. In investigations of the CHF using thin-films of other materials,[6, 9] the CHF approached an asymptotic limit as the thickness increased. In this study, we found that this asymptote occurred when the thickness of the graphene films was 150 nm.

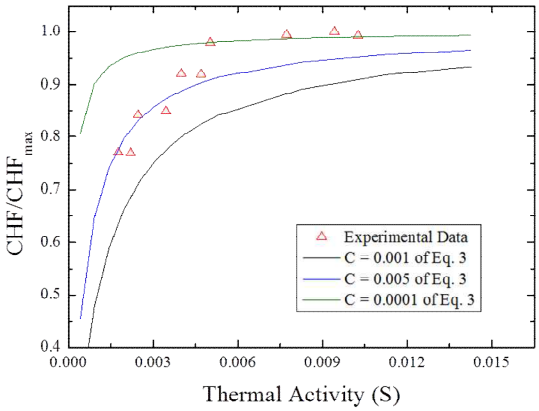

Fig. 5. The critical heat flux as a function of the thermal activity. [2]

The bare silicon and graphene-coated surfaces were visualized during boiling at 98% of the CHF using a high-speed IR camera (**Figure 6**). A large dry area (shown by the bright region in the figure), which persisted for more than 100 ms, was observed on the bare silicon surface. This dry area appeared as a hot circular area, which expanded as the microlayer evaporated at the center. As the CHF is reached, such dry areas become too hot to be re-wetted.[9] The graphene-coated surface exhibited only nucleate boiling at the same heat flux. No large dry areas were observed on the graphene-coated surface at the same heat flux. The graphene film has a larger thermal activity, and so can more effectively dissipate heat in the lateral direction, so the CHF was larger on the graphene-coated surface. Lateral heat dissipation in the graphene film is related not only to the thermal conductivity of the graphene film, but also to the thickness in **Figure 3**. An increase in the thermal activity may inhibit the formation of hot/dry areas.

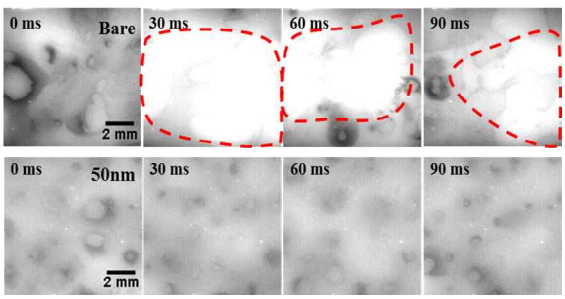

Fig. 6. IR images during boiling at 98% of the CHF bare surface and 50-nm-thick graphene-coated surface. [2]

Figures 7a and **7b** show IR images that compare graphene-coated heated surfaces of different thicknesses (and therefore different thermal activities). Large dry areas were less likely to appear and were shorter lived on the 50-nm-thick graphene-coated heated surface than

on the 15-nm-thick graphene-coated surface. The 50-nm-thick graphene film can dissipate heat at a greater rate than the 15-nm-thick graphene film, since the thermal activity is related to the thickness. Thus, lateral heat dissipation in the graphene film enhanced CHF.

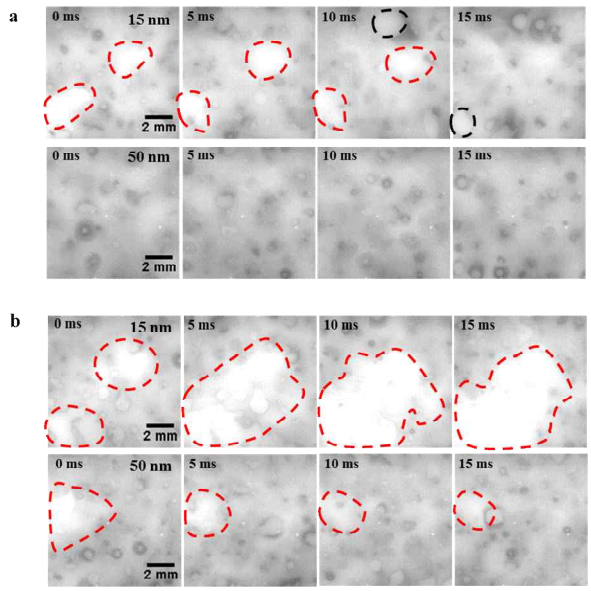

Fig. 7. IR images during boiling. **a.** The formation of dry areas on the 15- and 50-nm-thick graphene-coated surfaces at 80% of the CHF of the 15-nm-thick graphene-coated surface. **b.** The formation of dry areas on the 15- and 50-nm-thick graphene-coated surfaces at the CHF of the 15-nm-thick graphene-coated surface. [2]

Figure 8 shows temperature profile of the bare silicon and 50-nm-thick graphene-coated surfaces at 40% of the CHF of the bare silicon surface. The graphene-coated surface exhibited a larger nucleation site density and bubble frequency, with a smaller bubble diameter. These differences result from the surface characteristics of the graphene film, and lead to enhanced boiling performance, as shown in **Figure 3**.

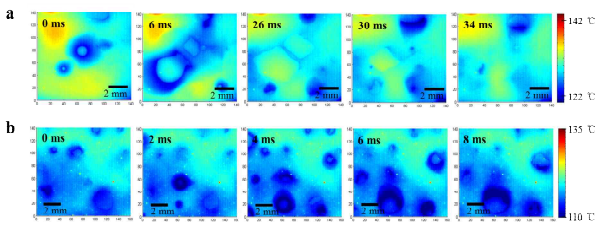

Fig. 8. IR image during boiling at 40% of the CHF of the bare silicon heater. **a.** Bare silicon surface. **b.** 50-nm-thick graphene film [2]

3. Conclusions

The graphene-coated heater showed an increase in BHT and CHF. As the thickness of the graphene films increased, the CHF also increased up to an asymptotic limit when the graphene layer was approximately 150 nm thick. The increased BHT was explained by the slight decrease in the wettability and the folded edges of the RGO flakes, which led to a decrease in the diameter of the departing bubbles, a larger bubble generation frequency, and an increase in the areal density of the bubble nucleation sites. The increase in the CHF was explained by considering the thermal activity of the graphene films, and the dependence thereof on the thickness and thermal properties of the layer, which was calculated based on high-speed IR visualization data.

REFERENCES

[1] Liang, Q., et al., *A three-dimensional vertically aligned functionalized multilayer graphene architecture: an approach for graphene-based thermal interfacial materials.* ACS nano, 2011. **5**(3): p. 2392-2401.
[2] Ahn, H. S., et al., *Enhanced Heat Transfer is Dependent on Thickness of Graphene Films: an Important Role of Graphene Film on The Heat Dissipation during Boiling*, submitted, 2014.
[2] Bae, S.-Y., et al., *Large-area graphene films by simple solution casting of edge-selectively functionalized graphite.* ACS nano, 2011. **5**(6): p. 4974-4980.
[3] Arik, M. and A. Bar-Cohen, *Effusivity-based correlation of surface property effects in pool boiling CHF of dielectric liquids.* International Journal of Heat and Mass Transfer, 2003. **46**(20): p. 3755-3764.
[4] Golobič, I. and A.E. Bergles, *Effects of heater-side factors on the saturated pool boiling critical heat flux.* Experimental thermal and fluid science, 1997. **15**(1): p. 43-51.
[5] Guglielmini, G. and E. Nannei, *On the effect of heating wall thickness on pool boiling burnout.* International Journal of Heat and Mass Transfer, 1976. **19**(9): p. 1073-1075.
[6] Jang, W., et al., *Thickness-dependent thermal conductivity of encased graphene and ultrathin graphite.* Nano letters, 2010. **10**(10): p. 3909-3913.
[7] Chai, L., M. Shoji, and X. Peng, *Dry patch interaction caused by lateral conduction in transition boiling.* International journal of heat and mass transfer, 2001. **44**(21): p. 4169-4173.
[8] Ma, K.-T. and C. Pan, *The effect of heated wall thickness and materials on nucleate boiling at high heat flux.* International communications in heat and mass transfer, 1999. **26**(8): p. 1103-1114.
[9] Wang, S., et al., *Wettability and surface free energy of graphene films.* Langmuir, 2009. **25**(18): p. 11078-11081.